








Article

Anti-Corrosion SiO_x-Doped DLC Coating for Raster Steel Linear Scales

Algirdas Lazauskas ^{1,*}, Viktoras Grigaliūnas ¹, Dalius Jucius ¹, Šarūnas Meškinis ¹,
Mindaugas Andrulevičius ¹, Asta Guobienė ¹, Andrius Vasiliauskas ¹ and Albinas Kasparaitis ²

¹ Institute of Materials Science, Kaunas University of Technology, K. Baršausko 59, LT-51423 Kaunas, Lithuania; viktoras.grigaliunas@ktu.lt (V.G.); dalius.jucius@ktu.lt (D.J.); sarunas.meskinis@ktu.lt (Š.M.); mindaugas.andrulevicius@ktu.lt (M.A.); asta.guobiene@ktu.lt (A.G.); andrius.vasiliauskas@ktu.lt (A.V.)

² JSC Precizika Metrology, Žirmūnų 139, LT-09120 Vilnius, Lithuania; a.kasparaitis@precizika.com

* Correspondence: algirdas.lazauskas@ktu.edu; Tel.: +370-671-73375

Abstract: In this study, we investigated the efficacy of SiO_x-doped diamond-like carbon (DLC) films for enhancing the corrosion resistance of raster steel linear scales. The research work highlights the significant role of DLC film materials in enhancing corrosion resistance, making them a promising solution for various industrial applications. The Raman spectroscopy analysis of SiO_x-doped DLC films, synthesized via a direct ion beam technique with HMDSO vapor, revealed prominent D and G bands characteristic of amorphous carbon materials, with a high degree of disorder indicated by an I_D/I_G ratio of 1.85. X-ray diffraction patterns confirmed the amorphous nature of the SiO_x-doped DLC films and the minimal impact of the DLC deposition process on the underlying crystalline structure of steel. UV–Vis–NIR reflectance spectra of SiO_x-doped DLC on stainless steel demonstrated improvements in the blue wavelength region compared to stainless steel with ripples alone, which is beneficial for applications utilizing blue light. Corrosion tests, including immersion in a 5% salt solution and salt spray testing, showed that SiO_x-doped DLC-coated stainless steel exhibited superior corrosion resistance compared to uncoated steel, with no significant signs of corrosion observed after extended exposure. These findings underscore the potential of SiO_x-doped DLC coatings to provide long-term corrosion protection and maintain the structural integrity and surface quality of steel components in harsh environments.

Keywords: SiO_x-doped DLC film; corrosion protection; raster steel linear scales



Citation: Lazauskas, A.; Grigaliūnas, V.; Jucius, D.; Meškinis, Š.; Andrulevičius, M.; Guobienė, A.; Vasiliauskas, A.; Kasparaitis, A. Anti-Corrosion SiO_x-Doped DLC Coating for Raster Steel Linear Scales. *Coatings* **2024**, *14*, 818. <https://doi.org/10.3390/coatings14070818>

Academic Editors: Luigi Calabrese and Edoardo Proverbio

Received: 12 June 2024

Revised: 26 June 2024

Accepted: 27 June 2024

Published: 1 July 2024



Copyright: © 2024 by the authors. Licensee MDPI, Basel, Switzerland. This article is an open access article distributed under the terms and conditions of the Creative Commons Attribution (CC BY) license (<https://creativecommons.org/licenses/by/4.0/>).

1. Introduction

Recently, a novel fabrication technique of raster steel linear scales (Figure 1) for reflective-type optical encoders was developed, applying ultrafast pico- and femto-pulse lasers to produce near-subwavelength ripples on polished stainless-steel tape. Careful selection of energy fluence near the ablation threshold [1] ensures that the ripples provide diffuse light reflection and high contrast compared to the well-reflecting steel gaps between the elements, thus ensuring the precision and reliability of the optical encoder measurements. Reliable displacement measurements are often required in harsh environments like marine, chemical, or food processing industries where steel corrosion phenomena can appear, especially in laser-fabricated ripple areas. It is well known that stainless steel corrosion resistance is determined by a very thin (1–3 nm) chromium oxide film [2], and the formation of ripples can affect the steel microstructure, which influences the corrosion resistance properties [3–5]. Ripples can create microenvironments on the surface of the oxide layer where local variations in pH, oxygen concentration, chemical composition, or other factors may occur, leading to localized corrosion, such as pitting or crevice corrosion, which can compromise the overall protective action of the oxide layer. Ripples may disrupt the continuity and integrity of the chromium oxide layer, exposing the underlying steel to the corrosive environment.

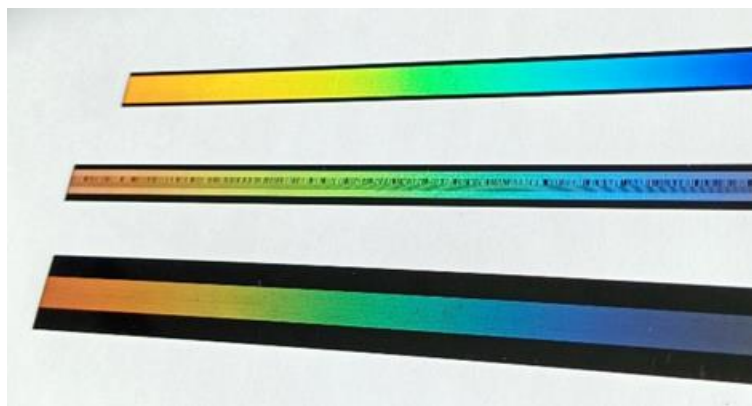


Figure 1. Raster steel linear scales for optical encoders.

Diamond-like carbon (DLC) coatings are known to have excellent anticorrosion properties because they are highly chemically inert and can withstand exposure to acids, bases, salts, and other corrosive agents without undergoing degradation [6–8]. By forming a dense and impermeable layer, DLC coatings prevent moisture, oxygen, and other corrosive species from reaching the underlying substrate and causing corrosion. The exceptional hardness and wear resistance of DLC coatings help to maintain the integrity of the coating even under abrasive conditions, reducing the risk of coating damage that could compromise corrosion protection. DLC coatings can be deposited on a wide range of substrate materials, including metals, ceramics, and polymers, making them versatile for corrosion protection applications in various industries [9,10]. DLC coatings offer comprehensive corrosion protection for steel by combining barrier properties, chemical inertness, surface passivation, hardness, wear resistance, and low friction characteristics [11–16].

In this work, we tested SiO_x-doped DLC coatings for corrosion protection of raster steel linear scales because these coatings offer key advantages compared to traditional DLC coatings [17–19]. The addition of SiO_x to DLC coatings increases their hardness and wear resistance, and they exhibit improved adhesion to steel substrates compared to those of pure DLC films [20–22]. This enhanced adhesion helps prevent delamination or spalling of the coating from the substrate, ensuring long-term protection against corrosion and wear [23–25]. Furthermore, the presence of SiO_x in DLC coatings enhances their chemical stability and resistance to degradation in harsh environments. SiO_x-doped DLC films are less susceptible to chemical attack from acids, bases, and other corrosive substances, providing superior corrosion protection for steel components exposed to aggressive operating conditions.

2. Materials and Methods

Near-subwavelength ripples (Figure 2) were fabricated on a hardened and tempered stainless steel tape SANDVIK 7C27Mo2–SGH CHROMFLEX (type AISI 420 + Mo) using picosecond laser beam irradiation ($\lambda = 532$ nm, $\tau_p = 8$ ps, laser fluence = 1.55 J/cm²).

Before deposition of the SiO_x-doped DLC film, the stainless-steel tapes were ultrasonically cleaned in fresh acetone (10 min) and isopropyl alcohol (10 min) at 35 °C to remove surface contamination. SiO_x-doped DLC films were deposited on the stainless-steel scales by a direct ion beam at room temperature using a closed-drift ion source. Hexamethyldisiloxane (HMDSO) vapor was used as a source of hydrocarbons, silicon, and oxygen. Hydrogen (H₂) was used as a carrier gas for HMDSO and was passed through the bubbler at a pressure of 450 Torr. The detailed deposition conditions of SiO_x-doped DLC films are given in Table 1.

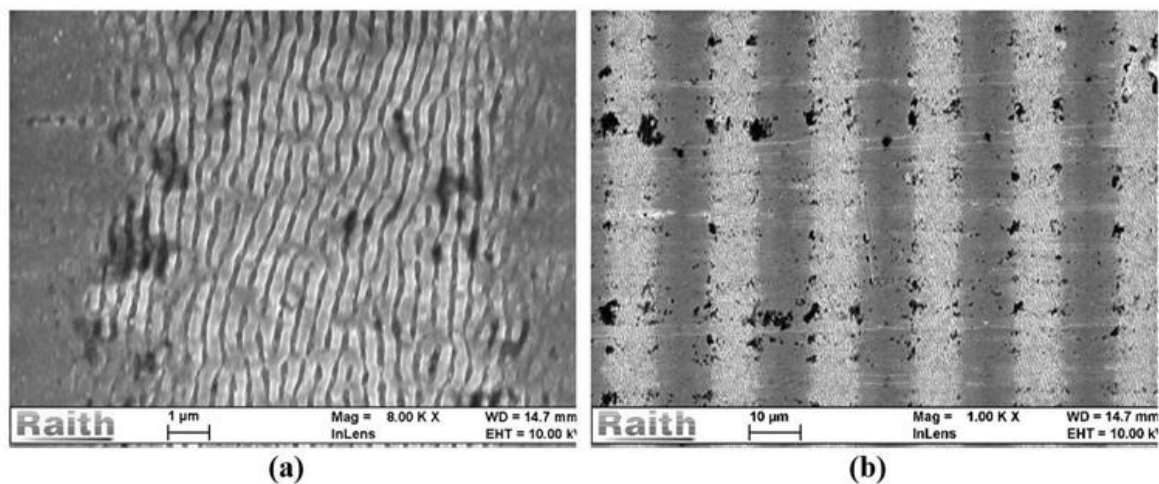


Figure 2. SEM images of near-subwavelength ripple areas under different magnifications: (a) 8000× and (b) 1000×.

Table 1. Deposition conditions of the SiO_x-doped DLC films.

Substrate	Stainless Steel
Reagents	Hexamethyldisiloxane (C ₆ H ₁₈ Si ₂ O) + H ₂
Base pressure	2 × 10 ⁻⁴ Pa
Work pressure	2 × 10 ⁻² Pa
Ion beam energy	1000 eV
Ion beam current density	50 μA/cm ²
Deposition time	10 min

The thickness and refractive index of the deposited films were measured by a laser ellipsometer Gaertner L115 ($\lambda = 633$ nm).

X-ray photoelectron spectroscopy (XPS) measurements were conducted using an XSAM800 spectrometer manufactured by Kratos Analytical Ltd., Manchester, United Kingdom (Kratos Analytical Ltd., Manchester, UK). XPS spectra were acquired utilizing non-monochromatized Al K α radiation ($h\nu = 1486.6$ eV).

Stainless steel scales with laser-fabricated ripples were characterized by the scanning electron microscope e-LiNEplus (Raith GmbH, Dortmund, Germany) and the atomic force microscope NanoWizard[®] 3 (JPK Instruments AG, Bruker Nano GmbH, Berlin, Germany). Corrosion behaviour was analyzed using a calibrated optical microscope B-600MET (OPTIKA Srl, Ponteranica, Italy) with a digital CCD video camera, Optika[™] Vision Pro (OPTIKA Srl, Ponteranica, Italy).

The crystallographic nature of the stainless steel and SiO_x-doped DLC film coated stainless steel samples was determined using a D8 Discover X-ray diffractometer (Bruker AXS GmbH, Berlin, Germany) with a Cu K α ($\lambda = 1.54$ Å) X-ray source. Parallel beam geometry with a 60 mm Göbel mirror (i.e., an X-ray mirror on a high precision parabolic surface) was used. The primary side also had a Soller slit with an axial divergence of 2.5° and a slit of 1.0 mm. The secondary side had a LYNXEYE (1D mode) detector with an opening angle of 2.16° and a slit opening of 6.0 mm. The X-ray generator voltage and current were 40.0 kV and 40 mA, respectively. Coupled $\theta/2\theta$ scans were performed in the range of 30.0–90.0° with a step size of 0.043°, a time per step of 19.2 s, and an auto-repeat function enabled. Processing of the resultant diffractograms was performed with DIFFRAC.EVA V7 software.

Raman spectra were recorded using an inVia Raman spectrometer (Renishaw, Wotton-under-Edge, UK) equipped with a CCD camera and confocal microscope (50× objective). The Raman spectra were excited with 532 nm radiation from a semiconductor

green laser at 5% output power in order to avoid damaging the sample. The 2400 lines/mm grating was used to record the Raman spectra.

Optical characterization of the stainless steel and SiO_x-doped DLC film-coated stainless steel samples was performed employing UV–Vis–NIR spectroscopy. The reflectance spectra were measured in the wavelength range of 300 to 900 nm (measurement resolution of 1.4 nm) using the AvaSpec-2048 (Avantes, Apeldoorn, The Netherlands) optical spectrometer and the combined deuterium/halogen light source AvaLight-DHc (Avantes, Apeldoorn, The Netherlands). Reflectance was measured with the standard small-tip reflection probe FCR-7UVIR200-2-1.5 (Avantes, Apeldoorn, The Netherlands) at an angle of 90 degrees.

The salt spray test was carried out on stainless steel and SiO_x-doped DLC film-coated stainless steel samples with a 5% NaCl solution at 100% relative humidity at 35 °C, according to ASTM B117-03. Photographs of the samples were taken at regular 24-h intervals over a 72-h period of the experiment to document their condition. Additionally, two sets of samples, one of uncoated stainless steel and the other of SiO_x-doped DLC film-coated stainless steel, were immersed in a 5% NaCl solution at room temperature. Images of each sample were taken at ten equally spaced time intervals over a 24-h period. The corroded area percentage was visually estimated from these images to quantify the extent of corrosion over time.

3. Results and Discussion

Figure 3 shows the X-ray diffraction (XRD) patterns of the stainless-steel sample (black pattern) and the SiO_x-doped DLC film deposited on the same steel (red pattern). The XRD pattern for the AISI 420 stainless steel exhibits peaks at 44.845°, 65.074°, and 82.358°, which correspond to the (1 1 0), (2 0 0), and (2 1 1) crystallographic plane orientations of a body-centered tetragonal (BCT) structure (ICDD PDF # 00-044-1289), confirming the presence of the full martensitic phase [26], with the space group *I4/mmm*. This XRD pattern indicates the complete transformation of steel to the martensitic phase, with no observable retained austenite or carbide phases. For the SiO_x-doped DLC film coated AISI 420 stainless steel, the XRD pattern shows peaks at 44.878°, 65.113°, and 82.356°, which align with the same BCT crystallographic plane orientations as the uncoated sample. This slight shift in peak positions suggests the introduction of residual stresses due to the SiO_x-doped DLC film coating process. The refined lattice parameters for the uncoated and SiO_x-doped DLC-coated stainless steel samples are nearly identical, with the values for the uncoated steel being $a = 2.860 \text{ \AA}$ and $c = 2.828 \text{ \AA}$, while the DLC-coated steel shows $a = 2.858 \text{ \AA}$ and $c = 2.829 \text{ \AA}$. The slight differences indicate minimal impact from the DLC deposition process, suggesting that the crystalline structure of the underlying steel remains largely unaffected. The absence of additional peaks in the XRD pattern of the SiO_x-doped DLC film-coated sample confirms that the SiO_x-doped DLC film is amorphous. This observation is in line with previous studies, which have consistently shown that SiO_x-doped DLC films do not exhibit crystalline peaks due to their amorphous carbon structure [27]. The amorphous nature of SiO_x-doped DLC film is known to enhance tribological properties, such as wear resistance and friction reduction, by providing a smooth and hard surface layer [28,29].

The Raman spectrum of SiO_x-doped DLC film, synthesized using a direct ion beam technique at room temperature with HMDSO vapor as the precursor, is shown in Figure 4. The spectrum displays two prominent peaks characteristic of amorphous carbon materials, identified as the D and G bands, located at approximately 1427 cm⁻¹ and 1507 cm⁻¹, respectively. The deconvolution of these bands shows that the D band, associated with sp³ carbon atoms in rings, has a larger area and width compared to the G band, associated with sp² carbon pairs in both rings and chains. The intensity ratio I_D/I_G was found to be 1.85, indicating a significant degree of disorder within the carbon network. The broader bands, with widths of 167 cm⁻¹ for the D band and 126 cm⁻¹ for the G band, are associated with a higher degree of disorder and a more significant presence of sp³ hybridized carbon [30]. The

peak positions suggest that the incorporation of SiO_x influences the bonding environment, with the G band shift towards a higher wavenumber indicating the decrease in the fraction of sp^3 bonds and the formation of more six-ring-like sp^2 clusters [31–33]. The high R-squared value (0.9939) confirms the reliability of the peak fitting and subsequent analysis.

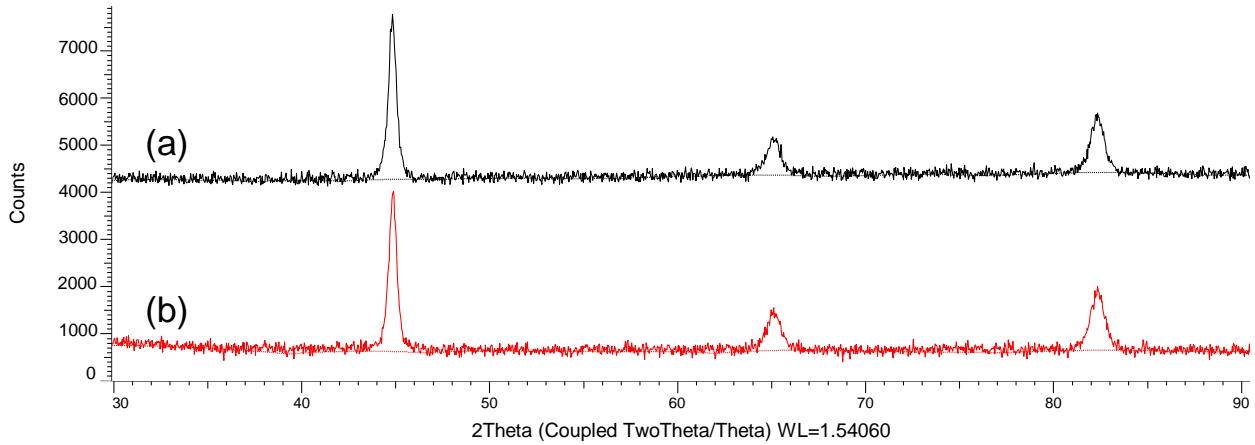


Figure 3. XRD patterns of stainless steel (a) and SiO_x -doped DLC film-coated stainless steel (b) samples.

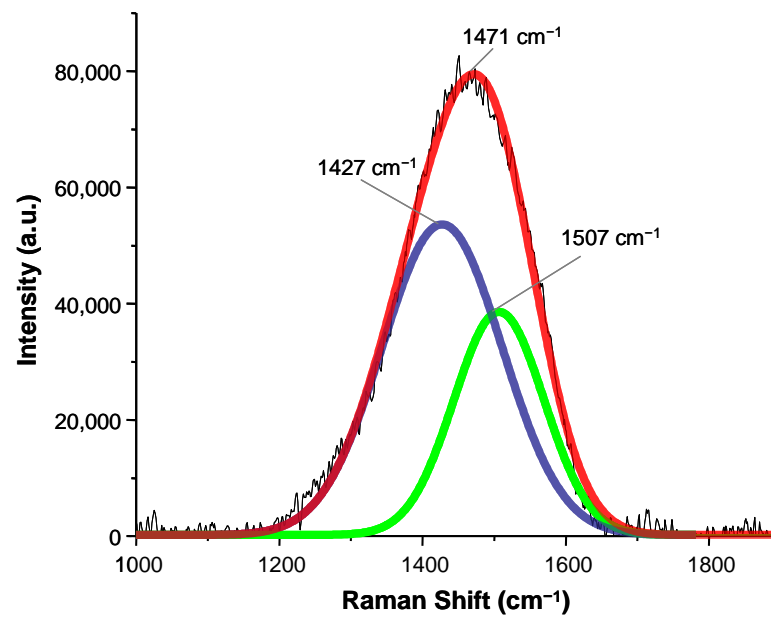


Figure 4. Raman spectrum of the SiO_x -doped DLC film. The blue and green lines show the deconvoluted D and G bands, respectively.

The average values of thickness and refractive index of the SiO_x -doped DLC film, measured by the laser ellipsometer, were found to be 80 nm and 1.88, respectively.

The XPS survey spectrum and calculated surface atomic concentrations of SiO_x -doped DLC film are shown in Figure 5 and Table 2, respectively. The composition analysis indicated that oxygen (O 1s) constituted 27.27% and silicon (Si 2p) was present at 20.44%. These results suggest a significant presence of oxygen and silicon dopants in the DLC film.

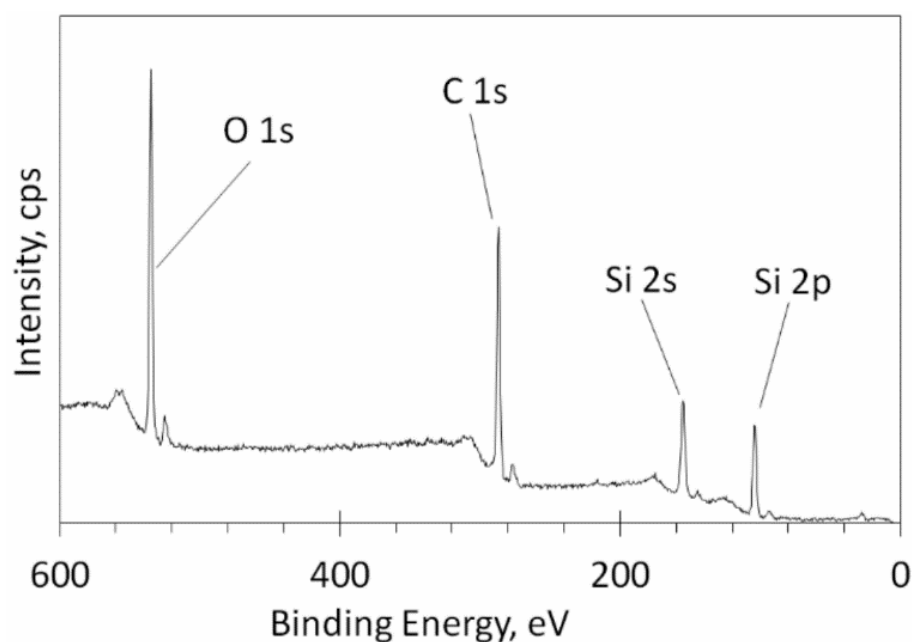


Figure 5. XPS survey spectrum of SiO_x-doped DLC film.

Table 2. Calculated surface atomic concentrations of the SiO_x-doped DLC films.

O 1s	C 1s	Si 2p
27.27%	52.29%	20.44%

A quantitative study of the surface morphology of stainless-steel scales was performed using an atomic force microscope. AFM topographic images and height profiles of stainless steel with ripples and SiO_x-doped DLC film on stainless steel with ripples are shown in Figure 6. Due to the increase in temperature, melting, and local material removal during the laser beam irradiation, clearly visible ripples with a period close to 450 nm and a height of 90 nm were formed on the surface of the steel tape (Figure 6a,c). The ripples were well defined and nearly parallel. The direct ion beam deposition of SiO_x-doped DLC films on stainless steel with ripples caused only minor changes in surface morphology (Figure 6b,d). Smoothing of the grooves during the coating process resulted in a decrease in the amplitude of the ripples on the DLC-coated scales to 80 nm. Thus, the amplitude change did not exceed 10 nm, and the ripples still had a significant influence on the scale surface roughness.

Figure 7 shows UV–Vis–NIR reflectance spectra of stainless steel, stainless steel with ripples, SiO_x-doped DLC film on stainless steel, and SiO_x-doped DLC film on stainless steel with ripples. The spectra reveal significant modifications in reflectance characteristics due to the presence of the SiO_x-doped DLC film. For uncoated steel (Figure 7a), the reflectance is highest, averaging 58.13%, with a reflectance range of 65%. This high reflectivity is typical of metallic surfaces. Introducing surface ripples (Figure 7b) reduces the reflectance to an average of 43.13% and narrows the range to 50% due to increased diffuse scattering caused by the textured surface. When a SiO_x-doped DLC coating is applied to steel (Figure 7c), the average reflectance decreases to 37.5%, with a range of 40%. The most significant reduction in reflectance is observed with SiO_x-doped DLC film on steel with ripples (Figure 7d), averaging 24.38% and exhibiting a reflectance range of 30%. Importantly, the SiO_x-doped DLC on stainless steel with ripples (Figure 7d) shows higher reflectance in the blue wavelength region compared to stainless steel with ripples alone (Figure 7b). This enhancement in the blue region is particularly beneficial for applications such as modern linear scale encoders [34–36], which exploit blue light due to its shorter wavelength and better photon penetration. Blue light improves the resolution and signal amplitude,

reduces harmonic distortion, and minimizes jitter, resulting in sharper imaging and higher precision. The reduced diffraction of blue light, as compared to red or infrared light, further accentuates these advantages.

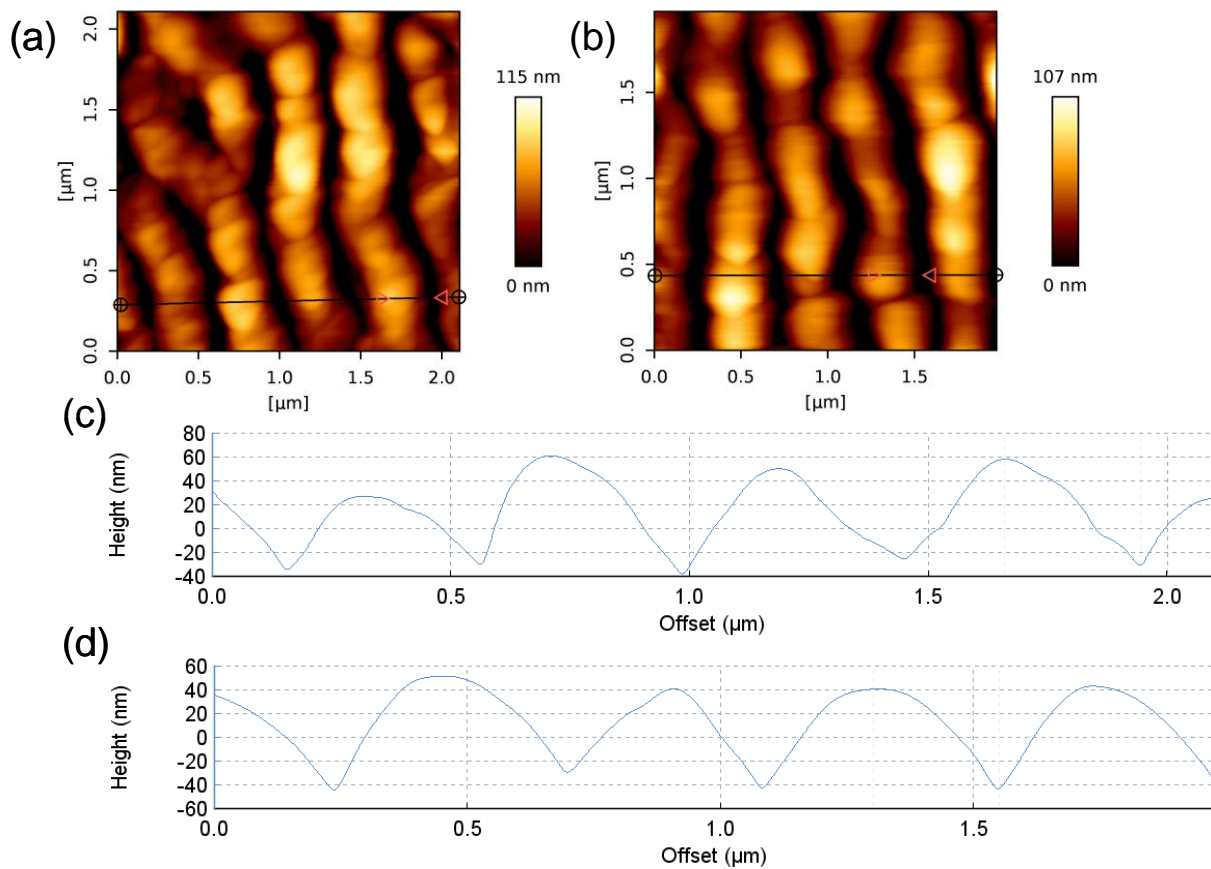


Figure 6. Topographic AFM images and height profiles of stainless steel with ripples (a,c) and SiO_x-doped DLC film on stainless steel with ripples (b,d).

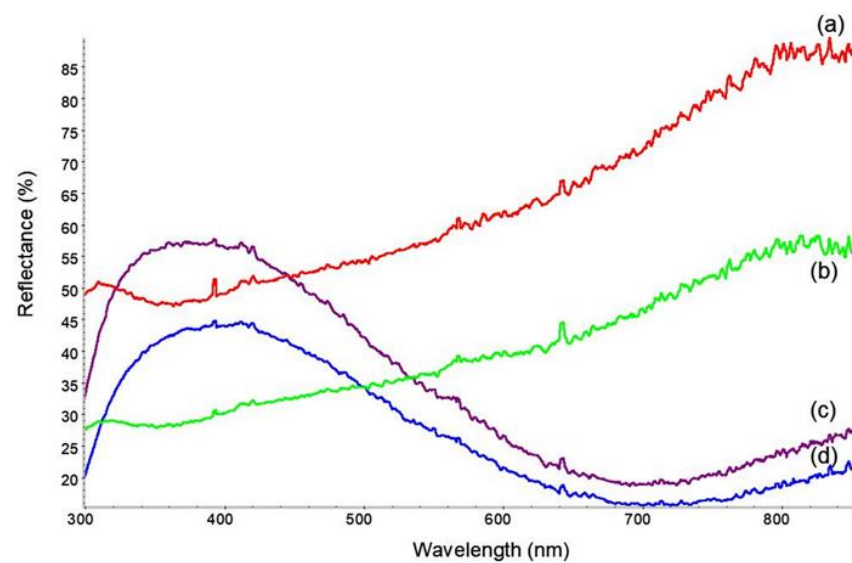


Figure 7. UV-Vis-NIR reflectance spectra of stainless steel (a), stainless steel with ripples (b), SiO_x-doped DLC film on stainless steel (c), and SiO_x-doped DLC film on stainless steel with ripples (d).

Corrosion is a pervasive issue affecting the longevity and performance of metallic materials, particularly in harsh environments such as those containing salt solutions. Figure 8 shows corrosion evolution on stainless steel and SiO_x-doped DLC film-coated stainless steel over a 24-h period of immersion in a 5% salt solution. The time-lapse images captured at regular intervals provide visual evidence of the corrosion processes, enabling a detailed comparative analysis.

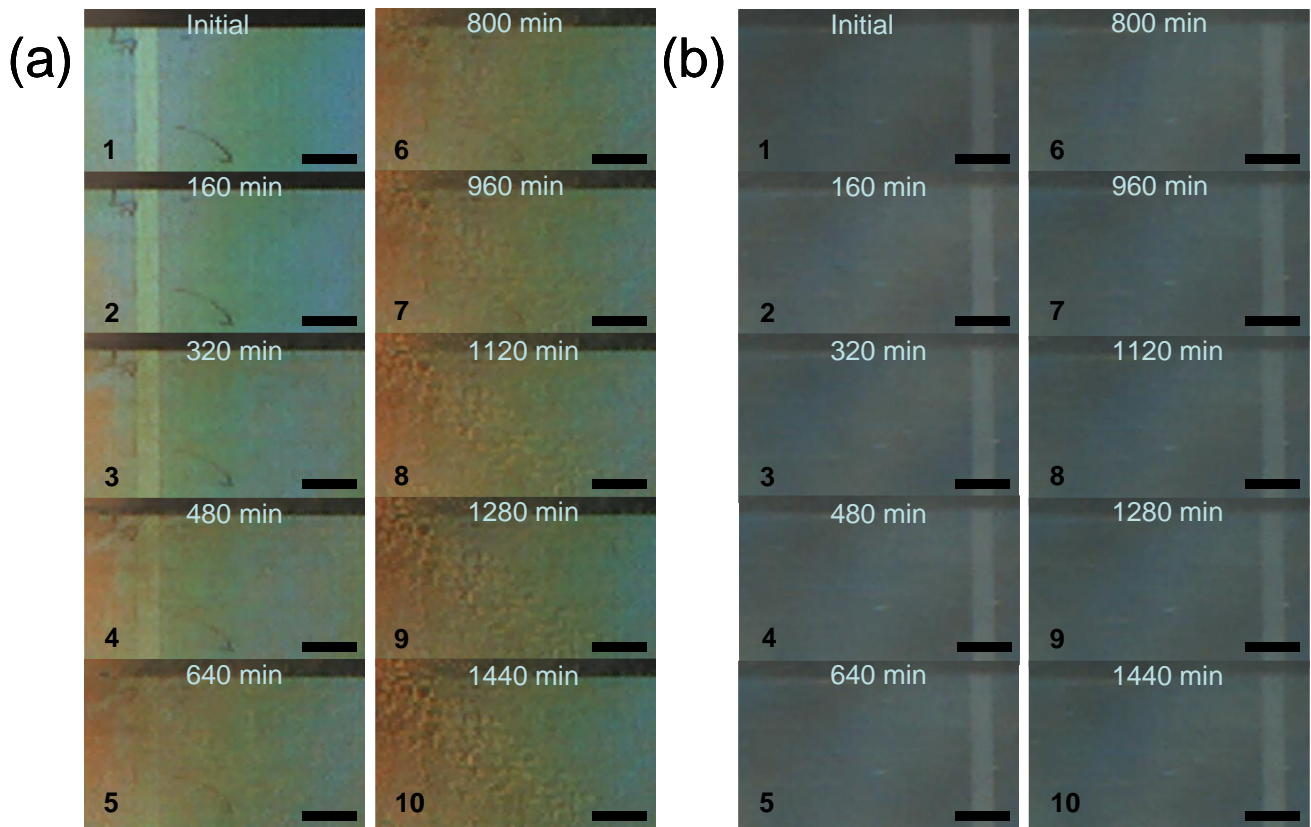


Figure 8. Corrosion evolution on stainless steel (a) and SiO_x-doped DLC film-coated stainless steel (b) over a 24-h period of immersion in a 5% salt solution. The time-lapse images were captured at regular intervals from 1 to 10. Mark size: 500 μm .

The images of the uncoated stainless-steel samples (Figure 8a) reveal a progressive and marked change in surface appearance due to corrosion. Initially (Figure 8a, time point from 1 to 5, 0–12 h) the sample exhibits a relatively uniform blue-green hue, indicative of light diffraction from raster ripples. However, early signs of corrosion appear as small brown spots, indicating the onset of rust formation. By the 12-h mark (Figure 8a, time point 5, 12 h), the corroded area expands to approximately 30% of the surface. Corrosion accelerates significantly in the later stages (Figure 8a, time point from 5 to 10, 12–24 h), with the corroded area covering 90% of the surface by the end of the 24-h period. The color transitions to a dominant brown, and the texture becomes rougher and more irregular, indicating severe degradation of the material. The early-stage (Figure 8a, time point from 1 to 5, 0–12 h) corrosion rate is calculated at 2.5% per hour, while the later-stage (Figure 8a, time point from 5 to 10, 12–24 h) rate escalates to 5% per hour, indicating accelerated corrosion progression.

The images of the SiO_x-doped DLC film-coated stainless steel sample (Figure 8b) demonstrate a stark contrast in corrosion resistance. The sample maintains a consistent greyish tone with no visible signs of corrosion during overall the 24 h period. This suggests that the SiO_x-doped DLC film coating effectively prevents the initiation of corrosion even in a saline environment.

Optical microscope images of the uncoated and SiO_x-doped DLC film-coated stainless steel surface over a 72-h period of the salt spray testing are presented in Figure 9. It is evident that the harsh test conditions cause notable surface corrosion of the uncoated stainless steel (Figure 9a). Degradation of the steel surface occurs in the form of localized pitting corrosion, starting at individual points and spreading laterally, forming brown spots that grow and eventually merge. In contrast, the SiO_x-doped DLC film-coated stainless steel surface (Figure 9b) demonstrates much greater resistance to corrosion. Over the 72-h period in the salt spray chamber, no significant signs of corrosion were observed on the surface of the SiO_x-doped DLC film-coated stainless steel. This confirms the suitability of SiO_x-doped DLC coatings for corrosion protection of stainless steel scales.

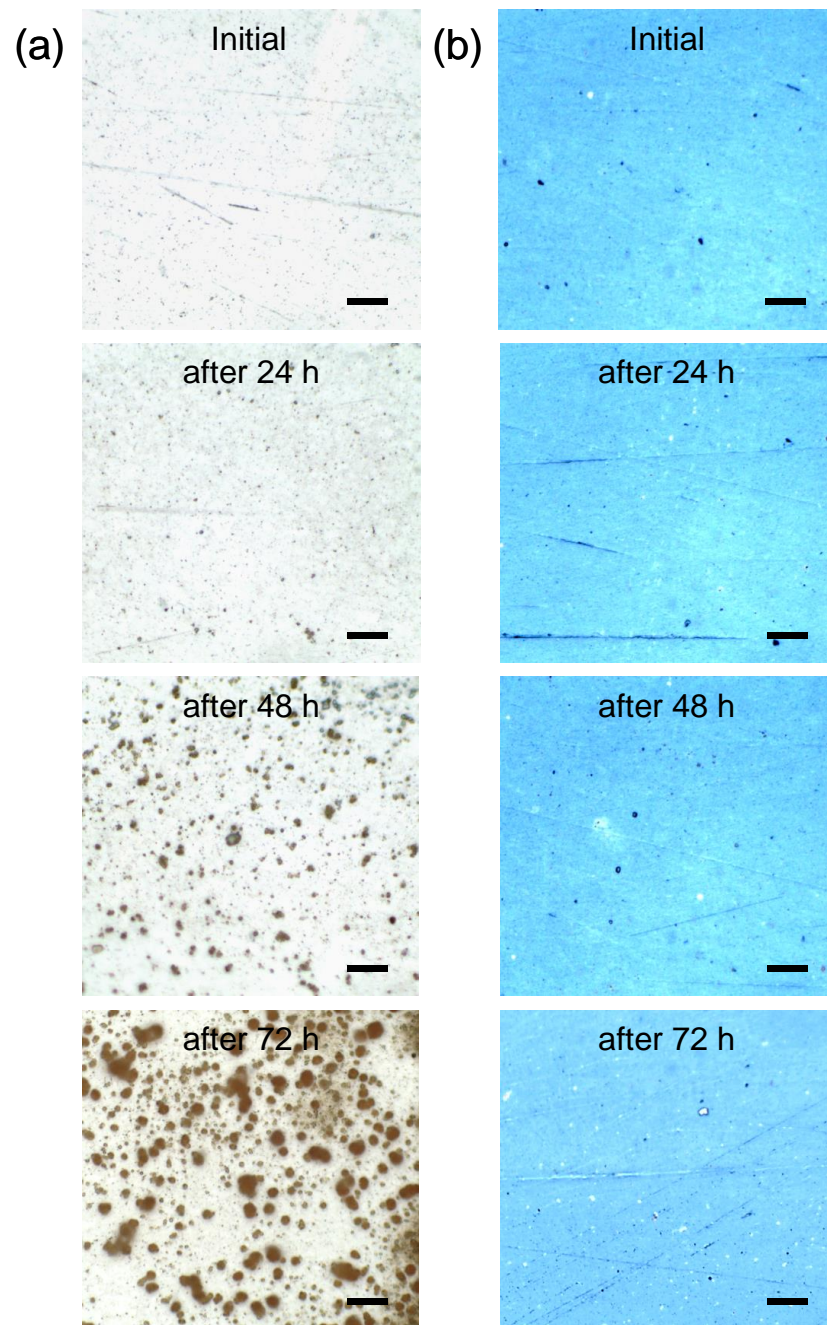


Figure 9. Corrosion evolution on stainless steel (a) and SiO_x-doped DLC film-coated stainless steel (b) over a 72-h period of salt spray testing. Optical microscope images were captured at regular 24-h intervals. Mark size: 20 μm .

These findings highlight the superior corrosion resistance provided by the SiO_x-doped DLC film coating, making it a highly effective solution for enhancing the durability of raster steel linear scales in corrosive environments. The SiO_x-doped DLC film-coated steel maintains its structural integrity and surface quality, showcasing the potential of such films in applications where corrosion resistance is critical.

4. Conclusions

This study demonstrates the effectiveness of SiO_x-doped diamond-like carbon (DLC) films for enhancing the corrosion resistance of raster steel linear scales. Raman spectroscopy displayed prominent D and G bands at 1427 cm⁻¹ and 1507 cm⁻¹, respectively. The intensity ratio I_D/I_G of 1.85 indicated significant disorder within the carbon network, with broader band widths (167 cm⁻¹ for the D band and 126 cm⁻¹ for the G band) suggesting a higher degree of sp³ hybridized carbon. The surface atomic concentrations of the SiO_x-doped DLC films for O 1s and Si 2p were found to be 27.27% and 20.44%, respectively. XRD analysis confirmed the amorphous nature of SiO_x-doped DLC film and indicated that the DLC deposition process did not significantly affect the crystalline structure of stainless steel. The SiO_x-doped DLC on stainless steel with ripples showed higher reflectance in the blue wavelength region compared to stainless steel with ripples alone, which is beneficial for applications utilizing blue light, such as modern linear scale encoders, improving resolution and signal quality. Time-lapse imaging in a 5% salt solution over 24 h revealed that uncoated stainless steel exhibited severe rust formation, with corroded areas covering 90% of the surface by the end of the period. In contrast, SiO_x-doped DLC-coated stainless steel showed no visible signs of corrosion, maintaining a consistent greyish tone throughout the 24-h period. After three days of salt spray testing, optical microscopy confirmed that the coated samples exhibited no significant signs of corrosion, unlike the heavily corroded uncoated samples. Overall, SiO_x-doped DLC coatings provide substantial improvements in chemical stability and corrosion resistance, making them ideal for applications requiring enhanced durability and reliability in aggressive environments.

Author Contributions: Conceptualization, V.G., A.K., and A.L.; investigation, D.J., A.L., Š.M., A.V., A.G., and M.A.; writing—original draft preparation, V.G., D.J. and A.L.; writing—review and editing, A.L., V.G., D.J., and Š.M.; visualization, A.L.; project administration, Š.M.; funding acquisition, Š.M. All authors have read and agreed to the published version of the manuscript.

Funding: This work was supported by the Research Council of Lithuania (Grant Number S-MIP-22-67).

Institutional Review Board Statement: Not applicable.

Informed Consent Statement: Not applicable.

Data Availability Statement: Data are contained within the article.

Conflicts of Interest: The authors declare no conflict of interest.

References

1. Ou, Z.; Huang, M.; Zhao, F. The fluence threshold of femtosecond laser blackening of metals: The effect of laser-induced ripples. *Opt. Laser Technol.* **2016**, *79*, 79–87. [[CrossRef](#)]
2. Santamaria, M.; Tranchida, G.; Di Franco, F. Corrosion resistance of passive films on different stainless steel grades in food and beverage industry. *Corros. Sci.* **2020**, *173*, 108778. [[CrossRef](#)]
3. Xu, Y.; Hou, X.; Shi, Y.; Zhang, W.; Gu, Y.; Feng, C.; Volodymyr, K. Correlation between the microstructure and corrosion behaviour of copper/316 L stainless-steel dissimilar-metal welded joints. *Corros. Sci.* **2021**, *191*, 109729. [[CrossRef](#)]
4. Zhang, T.; Zhou, B.; Wei, S.; Wang, Y.; Zhang, S. Effect of microstructure on the corrosion-friction behavior of low-carbon martensitic stainless steel. *Tribol. Int.* **2024**, *194*, 109560. [[CrossRef](#)]
5. Sun, M.; Xu, X.; Li, J.; Yang, L.; Liu, X.; Du, C.; Zhao, T.; Li, X. The influence of microstructures on the corrosion resistance of Cr-Mo-Sn low alloy steel in a tropical marine atmospheric. *Corros. Sci.* **2024**, *233*, 112058. [[CrossRef](#)]
6. Dearnaley, G.; Arps, J.H. Biomedical applications of diamond-like carbon (DLC) coatings: A review. *Surf. Coat. Technol.* **2005**, *200*, 2518–2524. [[CrossRef](#)]
7. Zhao, Q.; Mou, Z.; Zhang, B.; Zhang, X.; Wang, Z.; Wang, K.; Gao, K.; Jia, Q. Revealing the corrosion resistance of amorphous carbon films under heat shock via annealing. *Diam. Relat. Mater.* **2020**, *102*, 107692. [[CrossRef](#)]

8. Dalibón, E.; Escalada, L.; Simison, S.; Forsich, C.; Heim, D.; Brühl, S. Mechanical and corrosion behavior of thick and soft DLC coatings. *Surf. Coat. Technol.* **2017**, *312*, 101–109. [[CrossRef](#)]
9. Csorbai, H.; Kovach, G.; Pető, G.; Csikvari, P.; Karacs, A.; Solyom, A.; Hárs, G.; Kalman, E. Diamond–DLC double layer used in corrosive protective coating. *Appl. Surf. Sci.* **2007**, *253*, 5070–5075. [[CrossRef](#)]
10. Marin, E.; Lanzutti, A.; Nakamura, M.; Zanicco, M.; Zhu, W.; Pezzotti, G.; Andreatta, F. Corrosion and scratch resistance of DLC coatings applied on chromium molybdenum steel. *Surf. Coat. Technol.* **2019**, *378*, 124944. [[CrossRef](#)]
11. Radi, P.A.; Vieira, A.; Manfro, L.; de Farias Nass, K.C.; Ramos, M.A.R.; Leite, P.; Martins, G.V.; Jofre, J.B.F.; Vieira, L. Tribocorrosion and corrosion behavior of stainless steel coated with DLC films in ethanol with different concentrations of water. *Ceram. Int.* **2019**, *45*, 9686–9693. [[CrossRef](#)]
12. Hatada, R.; Flege, S.; Bobrich, A.; Ensinger, W.; Baba, K. Surface modification and corrosion properties of implanted and DLC coated stainless steel by plasma based ion implantation and deposition. *Surf. Coat. Technol.* **2014**, *256*, 23–29. [[CrossRef](#)]
13. Feng, X.; Hu, H.; Gui, B.; Guo, F.; Wang, K.; Zheng, Y.; Zhou, H. Corrosion behavior of W-DLC and DLC films deposited on plasma nitrided CF170 steel in H₂SO₄ solution. *Vacuum* **2022**, *204*, 111385. [[CrossRef](#)]
14. Ramos, B.; Vicente, F.; Hammes, G.; Bendo, T.; Binder, C. Enhancing corrosion and tribology performance of stainless steel with DLC coatings: Effects of doping and multilayered structures. *Surf. Coat. Technol.* **2024**, *477*, 130334. [[CrossRef](#)]
15. Zhang, T.; Deng, Q.; Liu, B.; Wu, B.; Jing, F.; Leng, Y.; Huang, N. Wear and corrosion properties of diamond like carbon (DLC) coating on stainless steel, CoCrMo and Ti6Al4V substrates. *Surf. Coat. Technol.* **2015**, *273*, 12–19. [[CrossRef](#)]
16. Nagai, T.; Hiratsuka, M.; Alanazi, A.; Nakamori, H.; Hirakuri, K. Anticorrosion of DLC coating in acid solutions. *Appl. Surf. Sci.* **2021**, *552*, 149373. [[CrossRef](#)]
17. Wei, X.; Feng, H.; Liu, Z.; Chen, Z.; Yin, P.; Lu, S.; Ding, J.; Du, N.; Li, X.; Zhang, G. Insight into the corrosion behaviors and mechanism of the self-healing Si/N-DLC films in oilfield environment. *Corros. Sci.* **2024**, *231*, 111989. [[CrossRef](#)]
18. Meškinis, Š.; Šlapikas, K.; Gudaitis, R.; Tamulevičius, S.; Kopustinskias, V.; Guobienė, A.; Niaura, G. SiOx-doped DLC films: Charge transport, dielectric properties and structure. *Vacuum* **2008**, *82*, 617–622. [[CrossRef](#)]
19. Meškinis, Š.; Tamulevičienė, A. Structure, properties and applications of diamond like nanocomposite (SiOx containing DLC) films: A review. *Mater. Sci.* **2011**, *17*, 358–370. [[CrossRef](#)]
20. Wu, X.; Suzuki, M.; Ohana, T.; Tanaka, A. Characteristics and tribological properties in water of Si-DLC coatings. *Diam. Relat. Mater.* **2008**, *17*, 7–12. [[CrossRef](#)]
21. Barve, S.; Chopade, S.; Kar, R.; Chand, N.; Deo, M.; Biswas, A.; Patel, N.; Rao, G.; Patil, D.; Sinha, S. SiOx containing diamond like carbon coatings: Effect of substrate bias during deposition. *Diam. Relat. Mater.* **2017**, *71*, 63–72. [[CrossRef](#)]
22. Kumar, N.; Barve, S.; Chopade, S.; Kar, R.; Chand, N.; Dash, S.; Tyagi, A.; Patil, D. Scratch resistance and tribological properties of SiOx incorporated diamond-like carbon films deposited by rf plasma assisted chemical vapor deposition. *Tribol. Int.* **2015**, *84*, 124–131. [[CrossRef](#)]
23. Grenadyorov, A.; Zhulkov, M.; Solovyev, A.; Oskomov, K.; Semenov, V.; Chernyavskiy, A.; Sirota, D.; Karmadonova, N.; Malashchenko, V.; Litvinova, L. Surface characterization and biological assessment of corrosion-resistant aC: H: SiOx PACVD coating for Ti-6Al-4V alloy. *Mater. Sci. Eng. C* **2021**, *123*, 112002. [[CrossRef](#)] [[PubMed](#)]
24. Yin, P.; Wei, X.; Shang, L.; Lu, Z.; Zhang, G. Design of low-friction and anti-corrosion aC: H: SiOx films. *Diam. Relat. Mater.* **2021**, *118*, 108512. [[CrossRef](#)]
25. Rajak, D.K.; Kumar, A.; Behera, A.; Menezes, P.L. Diamond-like carbon (DLC) coatings: Classification, properties, and applications. *Appl. Sci.* **2021**, *11*, 4445. [[CrossRef](#)]
26. Kadowaki, M.; Saengdeejing, A.; Muto, I.; Chen, Y.; Masuda, H.; Katayama, H.; Doi, T.; Kawano, K.; Miura, H.; Sugawara, Y. First-principles analysis of the inhibitive effect of interstitial carbon on an active dissolution of martensitic steel. *Corros. Sci.* **2020**, *163*, 108251. [[CrossRef](#)]
27. Mallik, A.K.; Dandapat, N.; Ghosh, P.; Ganguly, U.; Jana, S.; Das, S.; Guha, K.; Rebello, G.; Lahiri, S.K.; Datta, S. Deposition and characterization of diamond-like nanocomposite coatings grown by plasma enhanced chemical vapour deposition over different substrate materials. *Bull. Mater. Sci.* **2013**, *36*, 193–202. [[CrossRef](#)]
28. Wu, J.; Chen, L.; Ning, C.; Wu, G.; Lu, Z.; Shang, L.; Wu, Z.; Zhang, G. Tribo-mechanism of amorphous carbon films under corrosion solution and various mechanical loads. *Diam. Relat. Mater.* **2021**, *114*, 108318. [[CrossRef](#)]
29. Lazauskas, A.; Grigaliūnas, V.; Meškinis, Š.; Ecarla, F.; Baltrusaitis, J. Surface morphology, cohesive and adhesive properties of amorphous hydrogenated carbon nanocomposite films. *Appl. Surf. Sci.* **2013**, *276*, 543–549. [[CrossRef](#)]
30. Irmer, G.; Dorner-Reisel, A. Micro-Raman studies on DLC coatings. *Adv. Eng. Mater.* **2005**, *7*, 694–705. [[CrossRef](#)]
31. Xu, N.; Tsang, S.H.; Tan, C.W.; Teo, H.T.; Wang, X.; Tay, B.K. The effect of bonding structure of diamond like carbon (DLC) film with surface nickel coating upon laser annealing. *Prog. Nanotechnol. Nanomater.* **2013**, *12*, 35–39.
32. Kalish, R.; Lifshitz, Y.; Nugent, K.; Praver, S. Thermal stability and relaxation in diamond-like-carbon. A Raman study of films with different sp³ fractions (ta-C to a-C). *Appl. Phys. Lett.* **1999**, *74*, 2936–2938. [[CrossRef](#)]
33. Ferrari, A.C.; Robertson, J. Interpretation of Raman spectra of disordered and amorphous carbon. *Phys. Rev. B* **2000**, *61*, 14095. [[CrossRef](#)]
34. Quintián, F.P.; Calarco, N.; Lutenberg, A.; Lipovetzky, J. Performance of an optical encoder based on a nondiffractive beam implemented with a specific photodetection integrated circuit and a diffractive optical element. *Appl. Opt.* **2015**, *54*, 7640–7647. [[CrossRef](#)]

35. Wang, H.; Wang, J.; Chen, B.; Xiao, P.; Chen, X.; Cai, N.; Ling, B.W.-K. Absolute optical imaging position encoder. *Measurement* **2015**, *67*, 42–50. [[CrossRef](#)]
36. Lee, C.-H.; Huang, H.-J.; Chang, J.-P.; Chen, Y.-C. Incremental optical encoder based on a sinusoidal transmissive pattern. *IEEE Photonics J.* **2021**, *14*, 1–6. [[CrossRef](#)]

Disclaimer/Publisher’s Note: The statements, opinions and data contained in all publications are solely those of the individual author(s) and contributor(s) and not of MDPI and/or the editor(s). MDPI and/or the editor(s) disclaim responsibility for any injury to people or property resulting from any ideas, methods, instructions or products referred to in the content.